Dynamics Study of the Reaction Ar + HCN → Ar + H + CN

S. P. J. Rodrigues and A. J. C. Varandas*

Departamento de Química, Universidade de Coimbra, P-3049 Coimbra, Portugal

Received: March 11, 1998; In Final Form: May 18, 1998

A dynamics study of the reaction Ar + HCN → Ar + H + CN for a wide range of initial vibrational and translational energies is reported. All calculations have been carried out with the quasiclassical trajectory method and a realistic potential energy surface for ArHCN. An attempt is made to reproduce the thermal rate coefficient for the reaction. Agreement with experiment is found to be good, and the limitations of the approach are stressed. A brief analysis of rotational effects, energy transfer, and unimolecular dissociation of highly excited HCN* molecules is also presented.

1. Introduction

Unimolecular dissociation and the reverse recombination process are an important class of elementary reactions involved in combustion chemistry. According to the Lindemann approach and its subsequent refinements, namely, the extensively tested and widely accepted[1] Rice−Ramsperger−Kassel−Marcus (RRKM) scheme, such reactions become pressure-dependent in the so-called low-pressure limit (LPL), which is attained when the collisional excitation and deexcitation processes are dominant. At high temperatures reached in the flames, these processes govern the kinetics and the LPL rate constants become very important to rationalize such reactions. Furthermore, if Ar is assumed to be a representative example of a closed-shell third body, then the title reaction is of major importance for studying the propellant combustion reactions and, more generally, the combustion of nitrogen-containing materials at high temperatures.[2] Although these reactions have not been considered in the classical article of Miller and Bowman[3] on modeling the combustion chemistry of nitrogen compounds (they considered only temperatures up to 2500 K), for high temperatures the HCN removal by dissociation is expected to be competitive with oxidation by atomic oxygen.

Although widely used to rationalize mechanisms and evaluate rates, the RRKM framework is not yet predictive. The most severe and essential difficulty of RRKM theory is the need to specify a collision efficiency, or mean collisional energy transfer, quantities that cannot be obtained independentely. With this drawback, the RRKM rate constants must be calculated by using "typical" values for such quantities, often obtained from related systems for which the rate was fitted to experimental results. Of course, this may occasionally lead to the use of unrealistic values for the mean collisional energy.

The goal of the present work is to study theoretically the dynamics of the title reaction. The model is dynamical, and the thermal rate coefficient is calculated avoiding the usual energy transfer-based master equation formulation. The following fundamental assumptions are made: (a) the reaction occurs only on the ground potential energy surface of ArHCN, (b) the model potential energy surface describes accurately the reactive paths, (c) the classical trajectory method is adequate for studying the title reaction, (d) below the classical dissociation limit the HCN molecules are in thermal equilibrium, and (e) the density of states $\rho(E)$ can be described by a classical continuous function which can be approximated by using the harmonic approximation. We have found these assumptions acceptable, with (d) and (e) being the most problematic, as will be discussed later. An extra assumption concerns the definition of the HCN internal energy: (f) the internal energy of HCN is taken to be only vibrational. Thus, the angular momentum component perpendicular to the molecular axis is assumed to be vanishingly small, which implies that the trajectories begin with no rotational energy. Nevertheless, since this molecule is linear, a vibrational angular momentum l will appear.[4] This fact has been taken into account in the classical trajectory calculations by making a microcanonical sampling of the internal energy that has been distributed through the four normal modes of vibration: the degenerate bending modes and the two stretching ones.

The plan of the paper is as follows. In section 2 we describe the potential energy surface used for ArHCN. Section 3 presents the method used for the dynamics calculations. The technical details used for running the quasiclassical trajectories and the definition of the reactive channels are then examined. Section 4 is devoted to the theoretical framework utilized to calculate the thermal rate constant from the quasiclassical trajectories and to the analysis of the results. Rotational effects are also discussed in this section, where some remarks are made about the energy transfer in the title system. Similarly, the unimolecular dissociation of the HCN* complexes is briefly analyzed. Section 5 gathers the major conclusions.

2. Potential Energy Surface for ArHCN

To our knowledge, the only ab initio potentials available for the ArHCN van der Waals molecule are those of Clary et al.,[5] who have used the coupled electron-pair approximation (CEPA-1), and Tao et al.,[6] who have employed the Moller−Plesset (MP4) method. Both potentials have been fitted to analytical functions but the validity of these is restricted to the atom−rigid triatom Ar−HCN configurational regions. Other potentials have been reported[7−10] although the only six-dimensional (6D) is that of Bowman and co-workers.[9,10] This potential has been modeled by using Lennard-Jones pair potentials, which are known to be unrealistic in the inner repulsive wall. As this topographical feature can affect the dynamics,[11,12] the construction of a more realistic potential energy surface for ArHCN has been undertaken in the present work.

S1089-5639(98)01466-2 CCC: $15.00
Published on Web 07/10/1998

In this work, we write the 6D potential energy surface for ArHCN as the sum of a realistic double many-body expansion (DMBE) potential energy surface[13] for HCN with the relevant two-body potentials involving the argon atom. Thus,

$$V(\mathbf{R}) = V_{\mathrm{HCN}}(R_{\mathrm{CN}}, R_{\mathrm{CH}}, R_{\mathrm{NH}}) + \sum_{\beta=\mathrm{C,N,H}} V_{\mathrm{Ar}\beta}(R_{\mathrm{Ar}\beta}) \quad (1)$$

where **R** is a collective variable that denotes the six internuclear distances of the system. Similar pairwise models have been employed in dynamics studies of ArHCN,[9,10] and other systems such as ArO_3[14−16] and $ArHO_2$.[16−18] As stated above, the Lennard-Jones potentials are unrealistic and hence we have used the realistic Hartree−Fock approximate correlation energy[19,20] (generally denoted EHFACE) model, which is commonly employed in the DMBE[21] approach to represent the two-body potentials. For the argon interactions, it assumes the form[19−21]

$$V_{\mathrm{Ar}\beta}(R) = \lambda_{\mathrm{Ar}\beta} V_{\mathrm{HF}}(R) + V_{\mathrm{dc}}(R) \quad (2)$$

where $\lambda_{\mathrm{Ar}\beta}$ are scaling parameters that have been adjusted to obtain a satisfactory representation of the intermolecular Ar−HCN potential. The short-range Hartree−Fock-type energy has been written as a Born−Mayer function:

$$V_{\mathrm{HF}}(R) = A \exp(-bR) \quad (3)$$

where A and b are parameters obtained from a fit to restricted open-shell Hartree−Fock (ROHF) ab initio calculations; these will be discussed below for the Ar−C and Ar−N interactions. For Ar−H, the parameters in eq 3 have been taken from ref 16. Finally, the dynamical correlation has been semiempirically modeled by the damped dispersion energy as

$$V_{\mathrm{dc}}(R) = -\sum_{n=6,8,10} \chi_n(R) \frac{C_n}{R_n} \quad (4)$$

where C_n denotes the dispersion energy coefficients, and $\chi_n(R)$ are the damping functions described elsewhere[22] (see also ref 13 for explicit expressions).

The ab initio ROHF calculations for the ArC and ArN diatomic systems have been carried using the GAMESS[23] suite of programs. The standard internal valence triple-zeta (TZV) basis set of GAMESS, augmented with two polarization functions, has been utilized. This basis consists of (13s10p2d)/[6s5p2d] for argon[24] and (11s6p2d)/[5s3p2d] for carbon and nitrogen.[25] The calculated ab initio points were then used to fit the A and b parameters in eq 3. The root-mean-squared deviations of the ArC and ArN fits to the ROHF data for bond distances $1.5 \leq R/a_0 \leq 6.0$ are, respectively, $(1.8 \times 10^{-3})E_h$ and $(6.7 \times 10^{-3})E_h$ if one considers only the data beyond $3.5a_0$. We summarize in Table 1 the numerical values of the least-squares parameters in eqs 3 and 4.

The ab initio data used to calibrate the Ar−HCN interaction potential through optimization of the $\lambda_{\mathrm{Ar}\beta}$ parameters are the CEPA energies of Clary et al.[5] Such a fit has been carried out by minimizing the root-mean-square deviation between the ab initio energies and the model potential constrained to the condition that the absolute minimum should occur at linear geometries. Clearly, the fit assumes that the correlation energy at short range can be taken as a simple fraction of the Hartree−Fock component, an approximation that has been successfully used in previous work[26] for the alkali dimers. Although the final interaction potential is clearly approximate, we believe that it provides a reasonable model on which to carry out the dynamics calculations for the title reaction. In fact, scattering calculations using a refined energy switching (ES) potential energy surface[27] have shown that the results based on the improved ES model are essentially indistinguishable from those reported in the present work. This is also corroborated by the results[11,28] for rare-gas + CS_2 systems, which have shown that the precise form of the attractive well is relatively unimportant in scattering dynamics. Such results[11,28] have further indicated that the inner repulsive wall can be the most important feature of the potential to play a role in the dynamics, which supports our decision of replacing the Lennard-Jones potentials by the more realistic EHFACE-type potential energy curves.

TABLE 1: Parameters in the Two-Body Potentials of Equations 2−4[a]

	ArH	ArC	ArN
C_6	20.0[b]	52.0[c]	39.9[d]
C_8	426[b]	1174[e]	784[e]
C_{10}	12300[b]	26 512[e]	20 175[e]
R_0	7.09[b]	7.569	6.915
A	61.94[b]	29.172	35.123
b	1.91[b]	1.7636	1.659
λ	0.2047	6.2907	1.3951

[a] All quantities are in atomic units except λ, which is unitless. [b] Taken from ref 16. [c] Estimated by using a semiempirical combination rule from the C_6 dispersion coefficients of Ar_2 (ref 19) and N_2 (ref 48). [d] Estimated by using a semiempirical combination rule from the C_6 dispersion coefficients of Ar_2 (ref 19) and C_2 (ref 49). [e] Calculated from the universal correlation of ref 21.

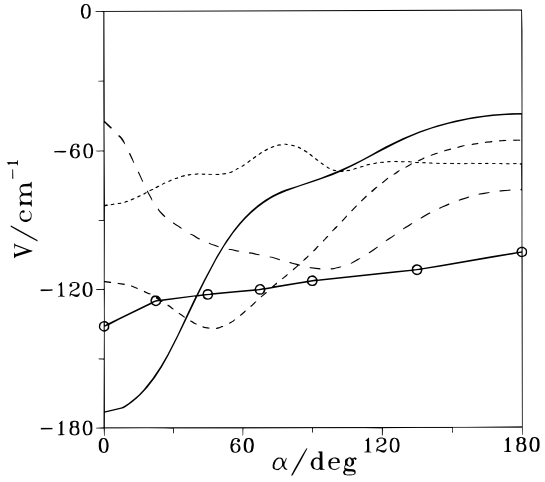

Figure 1. Minimum energy ArHCN potentials in atomic units: (—) this work; (•••) ref 5; (○) ref 6; (− − −) ref 8; (---) ref 9.

The final 6D potential energy surface (although all three-body energy terms involving the Ar atom are missing, it will be referred to hereafter as DMBE) has a linear minimum at −173.1 cm^{-1}, corresponding to a linear Ar−HCN geometry where $R_{\mathrm{ArH}} = 5.43a_0$ and HCN is at its equilibrium geometry. Such a well depth is larger than the available ab initio estimates[5,6] (−85.0 and −135.9 cm^{-1}, respectively) and required $\lambda_{\mathrm{Ar}\beta}$ parameters that differ significantly from unity. This fact reflects the lack of flexibility of the $\lambda_{\mathrm{Ar}\beta}$ parameters to fit the ab initio points, as can also be seen from Figure 1, which compares the minimum energy path of our DMBE potential energy surface with those of other potentials available in the literature. Despite the diversity of shapes and well depths, it is now a consensus[6,29] that the ArHCN complex is linear with a very flat angular potential around 90°. Clearly, the anisotropy of our ArHCN DMBE potential energy surface is overestimated, which causes large errors on the associated spectroscopic

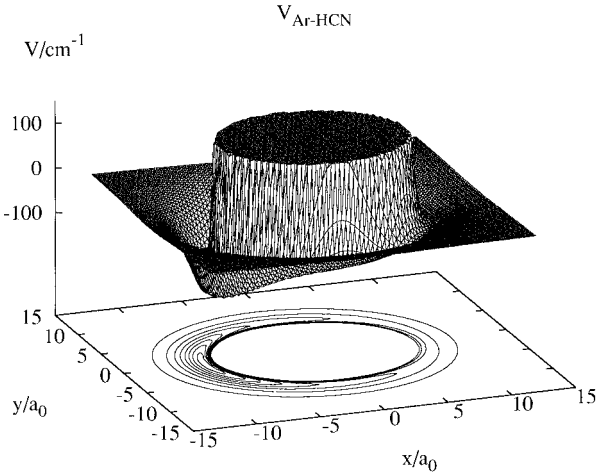

Figure 2. ArHCN potential energy surface for an Ar atom moving around an equilibrium HCN molecule.

properties.[27] However, as we have stated before, this fact has almost no influence on the dynamical properties of the title reaction.

A contour/perspective view plot of the ArHCN potential energy surface is shown in Figure 2 for the Ar atom moving around an equilibrium HCN molecule. It is seen that the DMBE potential energy surface is very smooth and shows no barriers for Ar approaching HCN except at short distances. We also observe that, from the point of view of reaction dynamics, the Ar approach to HCN is almost isotropic and is modeled essentially by the repulsive part of the potential energy surface.

3. Computational Method

The quasiclassical trajectory (QCT) method[30−32] is now a standard tool for carrying out studies of reaction dynamics. For the present QCT calculations we have used an extensively modified (see refs 16 and 18 for details) version of the MERCURY code.[33] A large set of batches of 10^3 trajectories has been run for different initial relative translational energies of Ar−HCN and vibrational energies of the HCN molecule in a total of 3.2×10^4 trajectories. The vibrational energy of HCN has been varied between 60 and 130 kcal mol^{-1} and distributed by using the microcanonical normal-mode sampling[34] scheme between the four vibrational normal modes of the molecule. In turn, the range of relative translational energies varied between 2 and 140 kcal mol^{-1}. This distribution leads to a cross section $\sigma(E_{tr},E_v)$, which depends on both the translational and vibrational energies.

The maximum impact parameter b_{max} has been optimized for each batch of trajectories from the requirement that no reactivity was detected in the last few bins for the selected channels in a total of 1000 trajectories. We have also imposed the more restrictive criterion that the chosen value of b_{max} would not lead to a significant energy transfer. The calculated optimum values (in angstroms) lie in the interval $3.6 \leq b_{max} \leq 5.6$ and are in the range of values reported[14,15,17,28,35,36] for other atom + triatom systems. Although as discussed by Bruehl and Schatz[11,37] the choice of b_{max} for energy transfer studies may lead to some ambiguity, such a problem is unimportant for the present study due to the fact that our main goals are the reactive rather than the energy transfer processes.

Assignment of Reactive Channels. The procedure employed to assign the reactive channels is identical to that reported by Varandas and co-workers[16,18] in studies involving the $ArHO_2$ and ArO_3 systems. The ArHCN system has 14 reactive channels

TABLE 2: Reactive Channels with Energies Referred to the ArHCN Minimum

channel no.	products	ΔE (kcal mol^{-1})
1	H + ArCN	130.99
2	Ar + HCN	0.498[a]
3	C + ArHN	229.68
4	N + ArHC	246.02
5	H + CN + Ar	131.16
6	H + C + ArH	311.43
7	H + C + ArN	311.80
8	H + N + ArC	311.79
9	Ar + C + NH	230.18
10	Ar + N + CH	246.49
11	ArH + CN	130.71
12	ArN + CH	246.41
13	ArC + NH	230.09
14	Ar + N + C + H	311.88

[a] Energetics of the HCN isomer.

(not counting the isomerization reaction); their assignment is made in terms of the energetics (reported in Table 2) and configurational properties (Table 3). We emphasize that only one channel is used to identify the HCN/HNC isomers. Their distinction is ambiguous for energies higher than the isomerization barrier and of little interest for the present study, although it can be made a posteriori by analyzing the results. The formation of HCN/HNC with energies higher than the threshold for H + CN dissociation (i.e., formation of a HCN* complex) has been analyzed a posteriori and considered as a distinct channel. Although in this case the configurational definition of the complex versus dissociated molecule may present some ambiguity, the subsequent dynamics study of its unimolecular dissociation can provide additional valuable information.[18,38]

4. Dynamics of the Reaction Ar + HCN → Ar + H + CN

The effect of pressure on the title reaction cannot be studied directly by the QCT method, which can only be used to study the title microscopic bimolecular process. Nevertheless, if the bimolecular reaction dominates over the unimolecular dissociation of HCN* in the low-pressure limit, the QCT method can indirectly provide valuable information about the reaction at the macroscopic level. Besides, the classical trajectory results from the present work suggest that the title bimolecular reaction proceeds through a mechanism that involves two routes for the dissociation process. First, an indirect route involving two stages: a metastable HCN* complex with energy above dissociation is formed:

$$\mathrm{Ar + HCN} \xrightarrow{k_1} \mathrm{Ar + HCN^*} \tag{5}$$

and then (note that the internal energy of the complex is above dissociation) the energized complex breaks up to form the products according to

$$\mathrm{HCN^*} \xrightarrow{k_2} \mathrm{H + CN} \tag{6}$$

Second, and less important, a route involving the formation of a very short-lived complex that dissociates promptly before the argon atom goes away:

$$\mathrm{Ar + HCN} \xrightarrow{k_3} \mathrm{Ar + H + CN} \tag{7}$$

As expected, both the direct formation of H + CN and the formation of HCN* contribute microscopically to the global thermal rate coefficient, which is given by $k = k_1 + k_3$.

TABLE 3: Definition of the Reactive Channels Used in the Trajectory Calculations for the ArHCN System[a]

channel no.	products	R_{CN} (Å)	R_{CH} (Å)	R_{ArC} (Å)	R_{NH} (Å)	R_{ArN} (Å)	R_{ArH} (Å)
1	H + ArCN	1.17	∞	4.30	∞	4.11	∞
		<1.40	>20.0	<5.16	>20.0	<4.93	>20.0
2	Ar + HCN[b]	1.17	2.17	∞	2.23	∞	∞
		<1.40	<2.56	>4.96	<2.68	>4.96	>4.96
3	C + ArHN	∞	∞	∞	1.04	3.83	2.79
		>6.35	>6.35	>6.35	<2.68	<4.93	<3.44
4	N + ArHC	∞	1.09	3.96	∞	3.83	2.87
		>5.99	<2.56	<5.16	>5.99	>5.99	<3.44
5	H + CN + Ar	1.17	∞	∞	∞	∞	∞
		<1.40	>5.00	>5.00	>5.00	>5.00	>5.00
6	H + C + ArH	∞	∞	∞	∞	∞	2.70
		>5.00	>5.00	>5.00	>5.00	>5.00	<3.44
7	H + C + ArN	∞	∞	∞	∞	4.41	∞
		>6.16	>6.16	>6.16	>6.16	<4.93	>6.16
8	H + N + ArC	∞	∞	4.30	∞	∞	∞
		>5.84	>5.84	<5.16	>5.84	>5.84	>5.84
9	Ar + C + NH	∞	∞	∞	1.04	∞	∞
		>5.84	>5.84	>5.84	<2.68	>5.84	>5.84
10	Ar + N + CH	∞	1.09	∞	∞	∞	∞
		>6.16	<2.56	>6.16	>6.16	>6.16	>6.16
11	ArH + CN	1.17	∞	∞	∞	∞	2.71
		<1.40	>5.00	>5.00	>5.00	>5.00	<3.44
12	ArN + CH	∞	1.09	∞	∞	4.11	∞
		>6.16	<2.56	>6.16	>6.16	<4.93	>6.16
13	ArC + NH	∞	∞	4.30	1.04	∞	∞
		>5.84	>5.84	<5.16	<2.68	>5.84	>5.84
14	Ar + N + C + H	∞	∞	∞	∞	∞	∞
		>6.35	>6.35	>6.35	>6.35	>6.35	>6.35

[a] The first entry specifies the configurational properties, while the second entry defines the actual geometries used. [b] The definition of this channel was chosen to include both HCN and HNC isomers.

Although it is reasonable to consider that a complex is formed whenever it lasts more than a few periods of vibration, a precise separation of the above two steps is somewhat arbitrary and hence conclusions taken from such a mechanism must be taken with care. On the other hand, the prevalent formation of HCN* over direct dissociation gives theoretical support to Lindemann-type macroscopic mechanisms for the overall reaction.

Thermal Rate Constant. The reactive cross section σ^r for a bimolecular reaction is given by

$$\sigma^r = \frac{N_r}{N_t}\pi\, {b_{max}}^2 \tag{8}$$

where N_r is the number of reactive trajectories, N_t is the total number of trajectories, and b_{max} is the maximum impact parameter. At the 68% confidence level, the error in σ^r is

$$\Delta(\sigma^r) = \sigma^r[(N_t - N_r)/N_t N_r]^{1/2} \tag{9}$$

A summary of the relevant QCT data and the calculated reactive cross section $\sigma(E_v,E_{tr})$ for the reactions in eqs 5 and 7 is shown in Table 4 where the estimated errors are also given. Figures 3 and 4 show the calculated reactive cross sections as a function of the translational energy for the various vibrational energies of HCN. As can be seen from Table 4 and Figures 3 and 4, the values of the reactive cross section for direct dissociation start to have significance only for total energies that are well above dissociation and are much smaller than those for HCN* complex formation. This is an expected result, which is similar to that obtained by Gallucci and Schatz[17] for He + HO_2. Due to the small collision times (<0.3 ps), the HCN* complexes do not have sufficient time to dissociate, and hence the trajectory finishes with HCN complex formation. On the other hand, direct dissociation appears to be caused by collisions having impact parameters with magnitude of the HCN dimensions as can be inferred from Figure 5, where the opacity functions for direct dissociation and formation of HCN* are shown for E_v = 130 kcal mol^{-1} and E_{tr} = 80 kcal mol^{-1}. For these initial conditions the average impact parameter $\langle b\rangle$ for direct dissociation is 1.9 Å, a value that is within the dimensions of a highly excited vibrational HCN molecule. Other initial vibrational and translational energies lead to similar results.

Clearly, an accurate fit of the calculated reactive cross sections to a bidimensional excitation function is a very difficult task due to the abrupt variation of the cross sections with vibrational energy near dissociation. Thus, we have instead chosen to carry out numerically the calculation of the thermal rate coefficient. This can be calculated from the reactive cross sections by averaging over the thermal distributions of translational and vibrational energies at a temperature T:

$$k(T) = \left(\frac{8kT}{\pi\mu}\right)^{1/2}\frac{1}{(kT)}\int_0^\infty\int_{E_0}^\infty E_{tr}\sigma(E_v,E_{tr})\rho(E_v)\times \exp[-(E_{tr}+E_v)/kT]\,dE_v\,dE_{tr} \tag{10}$$

To carry out the integrations in eq 10 we have employed the trapezoidal rule, with $\sigma(E_v,E_{tr})$ being evaluated by interpolation using the calculated discrete values. To warrant convergence, the translational energy values have been extrapolated, and the upper limit of integration over the vibrational energy has been taken as the dissociation energy. We have assumed this limit of integration because above dissociation one is in the energy regime for HCN* formation and hence should also account for the stabilization and unimolecular dissociation reactions. This would be a very difficult task, since one would then require an appropriate representation of the density of states (this may be nonthermal due to the rapid HCN* removal by unimolecular dissociation). In fact, trajectory calculations above dissociation show that a large amount of the initial HCN molecules (which

TABLE 4: Summary of the Trajectory Calculations for the Title Reaction[a]

E_{tr} (kcal mol^{-1})	E_{int}[b] (kcal mol^{-1})	b_{max} (Å)	N_c	σ_c (Å^2)	N_d	σ_d (Å^2)
100	60	3.6	5	0.20 ± 0.09	0	0
120	60	4.0	8	0.40 ± 0.14	0	0
140	60	4.0	17	0.86 ± 0.21	0	0
60	80	3.6	0	0	0	0
80	80	3.6	9	0.37 ± 0.12	0	0
100	80	3.8	21	0.95 ± 0.21	0	0
120	80	4.0	27	1.36 ± 0.29	0	0
50	100	3.6	17	0.69 ± 0.17	0	0
60	100	4.0	26	1.31 ± 0.25	0	0
80	100	4.0	47	2.36 ± 0.34	2	0.10 ± 0.07
100	100	4.0	70	3.52 ± 0.41	0	0
120	100	4.0	98	4.91 ± 0.45	2	0.10 ± 0.07
15	120	4.0	9	0.45 ± 0.15	0	0
20	120	4.0	32	1.61 ± 0.28	0	0
30	120	4.0	68	3.42 ± 0.40	3	0.25 ± 0.11
40	120	4.0	116	5.83 ± 0.51	4	0.20 ± 0.10
50	120	4.0	137	6.89 ± 0.55	3	0.15 ± 0.09
60	120	4.0	166	8.34 ± 0.59	9	0.45 ± 0.15
80	120	4.0	205	10.3 ± 0.6	14	0.70 ± 0.19
100	120	4.0	230	11.6 ± 0.7	25[c]	1.26 ± 0.25
120	120	4.0	241	12.1 ± 0.7	31[d]	1.56 ± 0.28
2	130	5.6	108	10.7 ± 1.0	3[e]	0.30 ± 0.17
5	130	5.6	184	18.1 ± 1.2	4	0.39 ± 0.20
10	130	5.6	250	24.6 ± 1.4	8[c]	0.79 ± 0.28
20	130	5.6	265	26.1 ± 1.4	15	1.48 ± 0.38
30	130	5.6	255	25.1 ± 1.4	27	2.66 ± 0.51
40	130	5.6	272	26.8 ± 1.4	33	3.25 ± 0.56
50	130	5.6	274	27.0 ± 1.4	37	3.65 ± 0.59
60	130	5.6	282	27.8 ± 1.4	35[b]	3.45 ± 0.57
80	130	5.6	273	26.9 ± 1.4	49[c]	4.83 ± 0.67
100	130	5.6	284	28.0 ± 1.4	43[c]	4.24 ± 0.63
120	130	5.6	277	27.3 ± 1.4	43[c]	4.24 ± 0.63

[a] The index c denotes the formation of unstable HCN*, while d represents the direct dissociative formation of H + CN. For all sets of translational E_{tr} and internal E_{int} energies, the number of integrated trajectories per batch has been 10^3. [b] Taken only as vibrational energy; see the text. [c] Including one trajectories that forms ArH + CN. [d] As in footnote *b* but including four trajectories. [e] As in footnote *b* but including two trajectories.

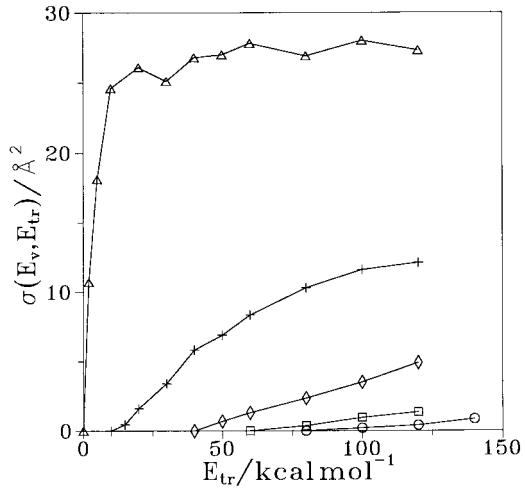

Figure 3. HCN* formation cross section as a function of translational and vibrational energies. Key for the symbols: (○) E_v = 60 kcal mol^{-1}; (□) E_v = 80 kcal mol^{-1}; (◇) E_v = 100 kcal mol^{-1}; (+) E_v = 120 kcal mol^{-1}; (△) E_v = 130 kcal mol^{-1}.

are in fact metastable HCN* complexes) dissociate before colliding with Ar. We illustrate one such trajectory in Figure 6. Gallucci and Schatz[17] have encountered a similar problem for the stabilization reaction of HO_2 by collision with He. However, they have considered only stabilized metastable HO_2

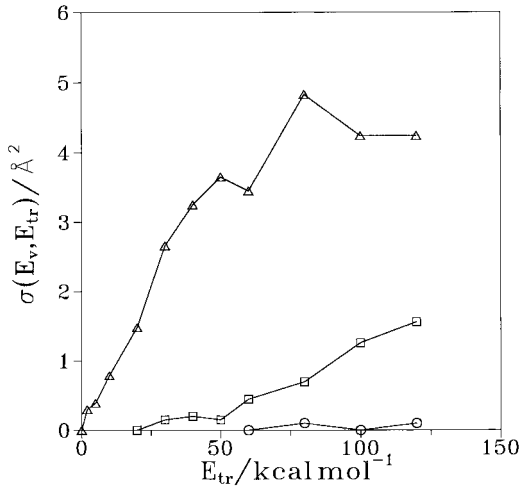

Figure 4. Cross section for direct formation of H+CN as a function of translational and vibrational energies. Key for the symbols: (○) E_v = 100 kcal mol^{-1}; (□) E_v = 120 kcal mol^{-1}; △, E_v = 130 kcal mol^{-1}.

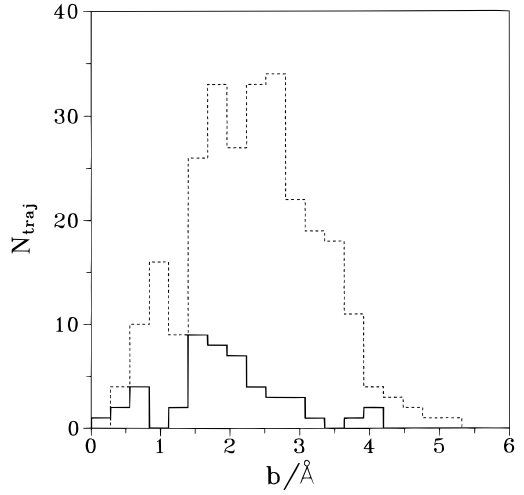

Figure 5. Opacity function for initial conditions E_v = 130 kcal mol^{-1}, E_{tr} = 80 kcal mol^{-1}, and b_{max} = 5.6 Å: (—) H + CN formation; (···) HCN* formation.

molecules and a constant density of states and hence avoided the unimolecular dissociation as well as the definition of the density of states.

Accurate calculations of the rovibrational levels of HCN have been reported by several authors[39−41] using variational methods and different potential energy surfaces. Unfortunately, these calculations have been carried out only for low total angular momenta ($J \leq 2$) and energies up to ca. 25 000 cm^{-1}, which means that the calculations were extended to high energies but always in the neighborhood of the isomerization barrier. Moreover, for energies higher than the isomerization barrier, not all calculated states appear to be converged or even detected. Clearly, to extend such calculations to energies just below dissociation (45 700 cm^{-1}) and to high total angular momenta (J) is an overwhelming task. Thus, the direct counting of accurate variationally calculated rovibrational states for HCN is out of question, and other methods must be sought to obtain the density of states.

In the present work, an analytical function for the density of vibrational states $\rho(E_v)$ has been used. Although the internal states of HCN are quantized, its density can be approximately described classically, especially for the high energies sampled in our study. In the present work we have represented the vibrational density of states by the analytical Marcus−Rice[42]

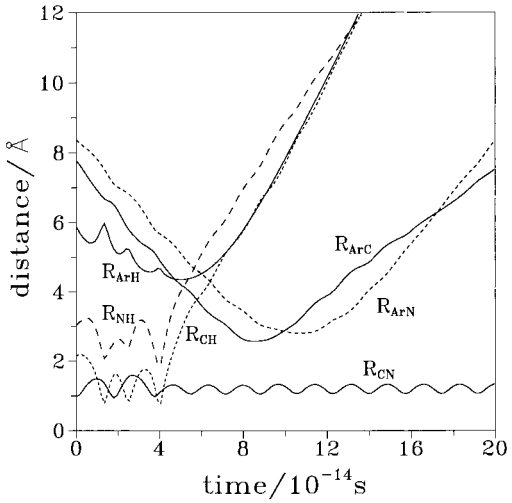

Figure 6. Internuclear distance vs time plot for a typical trajectory in which HCN dissociates before "colliding" with Ar. The initial conditions are $E_{tr} = 100$ kcal mol^{-1}, $E_v = 160$ kcal mol^{-1}, and $b_{max} = 5.6$ Å.

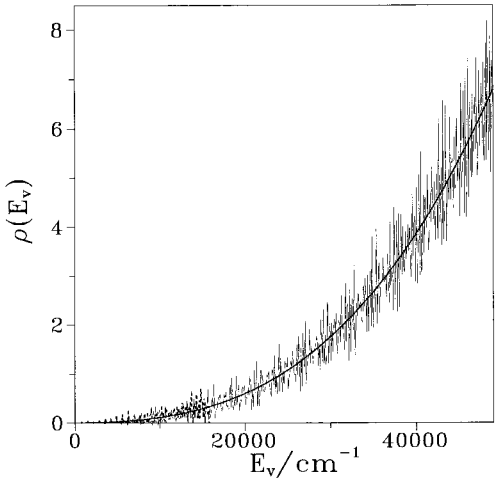

Figure 7. Density of vibrational states for HCN. The thin curve represents the "exact" counting of harmonic levels while the thick solid curve indicates the Marcus−Rice approximation. Shown by the thick dashed curve is the "exact" counting of the variationally calculated levels of ref 40.

formula:

$$\rho(E_v) = \frac{(E_v + E_z)^{s-1}}{(s-1)\prod \nu_i} \tag{11}$$

where

$$E_z = \sum_{i=1}^{s} \left(\frac{1}{2} h\nu_i\right) \tag{12}$$

and $s = 4$ is the number of vibrational frequencies of HCN; $\nu_1 = \nu_2 = 713$ cm^{-1}, $\nu_3 = 2097$ cm^{-1}, and $\nu_4 = 3312$ cm^{-1}. As seen from Figure 7, this expression gives an accurate density of harmonic states for the title system. It provides a good fit to the direct counting of harmonic states over the range of energies relevant for the present work, while agreeing well with the more elaborate Whitten−Rabinovitch formula.[43,44]

It should be stressed at this point that the use of the harmonic approximation to treat the vibrational states of HCN rather than counting the anharmonic ones directly is expected to be the most

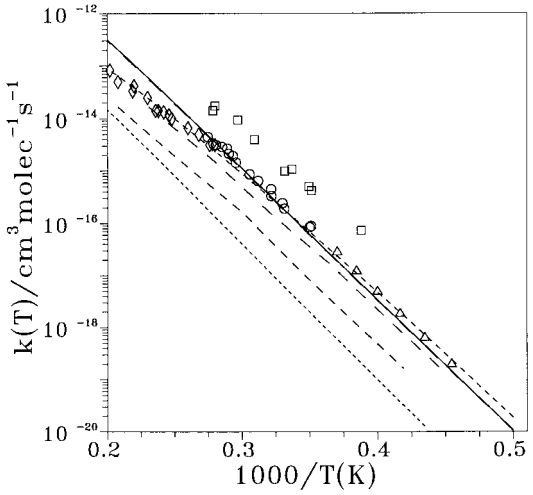

Figure 8. Thermal rate coefficient for the Ar + HCN → Ar + H + CN reaction. Theoretical results: —, this work ($k_1 + k_3$); ···, this work (k_3); --- and — — —, ref 50. Note that the calculated k_1 from the present work (which is shown by the long-dashed line), is nearly indistinguishable from the total rate constant (solid line). Experimental data: (□) Tabayashi et al.;[51] (△) Roth and Just;[52] (○) Szekely et al.;[53] (◇) Szekely et al.[54] (as cited in refs 2 and 50); (---) recommended, ref 2.

significant source of error in our calculation. Figure 7 compares the density of states used in the present work with other results. Also included for comparison in this figure are two nearly "exact" countings of states: the standard harmonic one and that based on the variational states reported by Bowman et al.[40] (these are expected to be accurate only up to ca. 18 000 cm^{-1}). In this case, the number of bending vibrational levels has been multiplied by the degeneracy of the corresponding harmonic level. These term frequencies can be calculated variationally from calculations for total angular momenta, $J = |l| = v, v - 2, ..., 0$ (or 1), and must appear split. However, the approximation used in the present work seems accurate enough for comparison purposes, given the deviations of the calculations from the experimental values and the accuracy of the density of states.

An estimate of the error in the present approach has to take into account the approximations of the method and the numerical errors of the calculations. The error from the QCT calculations and that due to the integration by the trapezoidal rule are estimated to be less than 10% and hence very small when compared to the error caused by the approximations in the density of states. A conservative estimate for the global error is probably a factor of 2, mainly due to the density of states.

Figure 8 shows the dependence on temperature of the calculated thermal rate coefficient, where the known experimental and theoretical results are also given. The agreement with experiment is good except for very high temperatures. The disagreement with experiment is then probably due to the use of rotationally cold molecules and the fact that one is not accounting for the expected nonthermal distribution near dissociation.

Rotational Effects and Energy Transfer. To gain some insight into the effect of rotational energy in the dynamics of the title reaction, we have performed two batches of trajectory calculations in which a thermalized rotational energy distribution has been taken for HCN (this corresponds to a mean rotational energy of $\langle E_r \rangle = 10$ kcal mol^{-1}); see Table 5. We have therefore assumed separation of vibration from rotation, with the rotational energy being distributed as $kT/2$ per symmetry axis of the molecule. To partition the vibrational energy, we have used the microcanonical sampling scheme.

TABLE 5: Comparison of the Trajectory Calculations for the Title Reaction with and without Inclusion of Rotational Energy[a]

E_{tr}	E_v	E_r	b_{max} (Å)	N_C	σ_C (Å^2)	N_D	σ_D (Å^2)
40	120	10	5.6	223	22.2 ± 1.3	9	0.90 ± 0.03
60	120	10	5.6	284	22.6 ± 1.3	16	1.59 ± 1.3

[a] The index c denotes the formation of unstable HCN*, while d represents the direct dissociative formation of H + CN. For all sets of translational E_{tr} and internal E_v and E_r energies in kilocalories per mole, the number of integrated trajectories per batch has been 10^3. Only 989 trajectories finished in 60 ps when rotation was included.

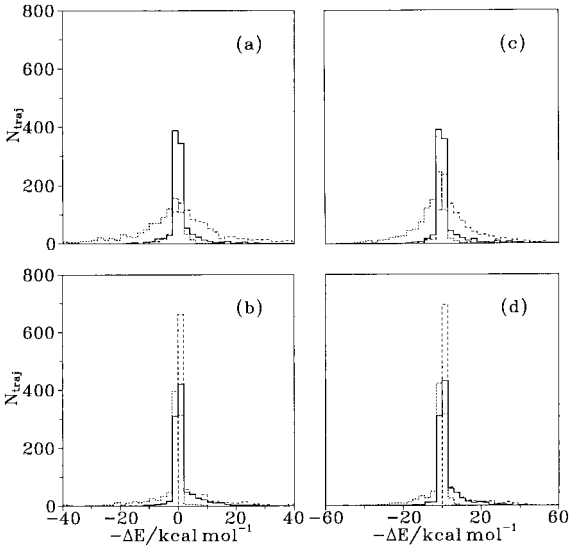

Figure 9. Frequency of energy transfers to the HCN molecule after collision with Ar. The initial total energy of HCN is 130 kcal mol^{-1}, which has been distributed as (a, c) 10 kcal mol^{-1} of initial rotational energy and 120 kcal mol^{-1} of initial vibrational energy; (b, d) 130 kcal mol^{-1} of initial vibrational energy and zero initial rotational energy. Initial translational energy: (a, b) $E_{tr} = 60$ kcal mol^{-1}; (c, d) $E_{tr} = 80$ kcal mol^{-1}. Key for the lines: (—) total internal energy; (•••) vibrational energy; (---) rotational energy.

In comparison with Table 4 (see entries 27 and 29 of this table), the data in Table 5 indicate that the inclusion of rotational energy leads to a decrease of the reactive cross section for the same total initial internal energy of HCN. Since this effect is expected to become more important at high temperatures, the error in the calculated thermal rate coefficient may be partly ascribed to rotational effects.

Turning now our attention to a detailed analysis of the rotational effects, one observes that at the beginning of the trajectories the HCN molecules are highly vibrationally excited and some of this energy is then transferred to rotation; of course, the overall energy gain comes from the transfer of translational energy from the colliding Ar atom. Figure 9 shows the energy transfer distributions of the HCN* complexes with and without rotational energy for specific initial conditions. We have followed the usual convention in which a negative energy transfer implies energy pumped to HCN. Although the separation of rotation from vibration is impossible for the high energies sampled, a large vibrational−rotational (V−R) internal energy transfer is apparent for all the conditions shown. Also visible in this figure are the very similar features of all curves, which appear to scale from $E_v = 40$ to 60 kcal mol^{-1}.

It is well-known[12,14,45] that the energy transfer calculated from trajectory results must be properly scaled to be compared with the experimental "per collision" results. For a proper canonical or microcanonical system using a sufficiently large maximum

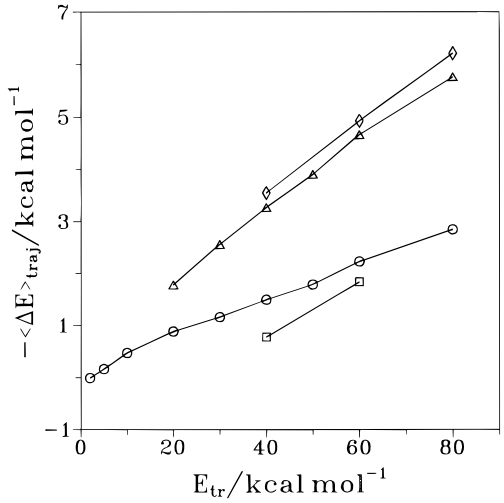

Figure 10. Average energy transferred per collision to the HCN molecule after collision with Ar as a function of the translational energy: (◇) $E_v = 100$ kcal mol^{-1}; (△) $E_v = 120$ kcal mol^{-1}; (○) $E_v = 130$ kcal mol^{-1}; (□) $E_v = 120$ kcal mol^{-1} with 10 kcal mol^{-1} of initial rotational energy.

impact parameter b_{max} and a large number of trajectories the calculated energy transfer $\langle\Delta E\rangle_{traj}$ is converged to a value that must be scaled by a physically reasonable constant,[45] e.g., $(b_{max}/d)^2$ where d is the hard-sphere radius of the molecule. In the present work, only the qualitative features of the microcanonical energy transfer will be analyzed and this multiplicative constant will not be used. The behavior of the energy transfer for some sets of HCN internal energies and relative translational energies of the complex is shown in Figure 10. It is seen that the amount of energy transferred increases monotonically with translational energy but diminishes with the internal vibrational energy of HCN. Nevertheless, one can note that the variation of the energy transfer for $E_v = 130$ kcal mol^{-1} shows a different rate of increase with E_{tr}, which can be attributed to the near-dissociation regime, where the capacity of the molecule to absorb energy is significantly diminished. We now address the results obtained with initial rotational energy, the interpretation of which must be made with some care since we have used in this case a mixed canonical/microcanonical calculation. There is clearly a decrease of the energy transfer relative to that observed for the same vibrational energy but with no rotation. A smaller decrease is also observed relative to the energy transfer for the same total energy (but all of vibrational type). We note that a similar decrease with rotational energy has also been reported by other authors[14,15] for analogous systems. This effect has been attributed[15] to the rotational−translational energy transfer that occurs when the molecule is rotating and that decreases the energy transfer from Ar to HCN. As far as we know, the decrease of energy transfer with initial vibrational energy was not analyzed in the literature. As seen from Figure 9, there is a large V−R energy transfer in the collisions, which leads to an increase of the rotational energy of the molecule.

Unimolecular Dissociation of the HCN* Complexes. The dynamics of the HCN* complexes with energy above dissociation can be used to estimate the microcanonical or canonical unimolecular decay rate HCN* → H + CN. Following previous work,[18] a brief discussion of their dynamics will be attempted. Thus, after the HCN* complexes have been formed, the trajectories were allowed to continue until dissociation occurs or a limiting time of 60 ps has been achieved. Figure 11 shows the logarithm of the HCN* decay rate as a function of time for some of the trajectory initial conditions. As in previous work

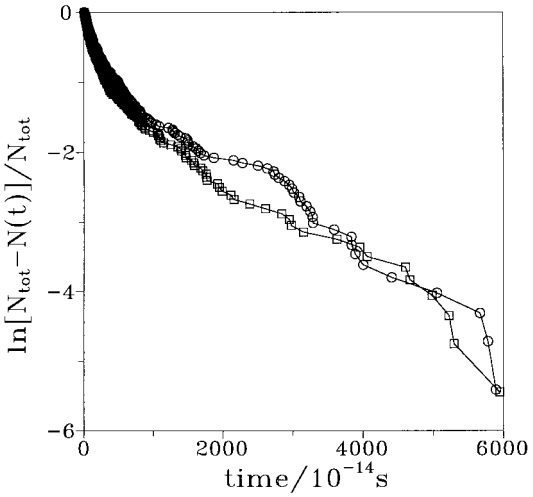

Figure 11. Logarithm of the decay rate of HCN* complexes as a function of time for initial vibrational energy $E_v = 130$ kcal mol^{-1}; (○) $E_{tr} = 60$ kcal mol^{-1}; (□) $E_{tr} = 80$ kcal mol^{-1}.

for HO_2[18] and O_3,[46] the energy distribution of these complexes does not form an exact microcanonical ensemble, although Figure 9 shows that the energy distribution peaks sharply around the average value of the internal energy. Thus, the observed near-linear dependence in Figure 11 suggests that the HCN* complexes have random lifetimes with the dissociation reaction following a RKRM-type behavior.[18,47]

5. Concluding Remarks

In the present work we have carried out a theoretical dynamics study of the reaction Ar + HCN → Ar + H + CN for a wide range of initial internal vibrational energies of HCN and initial relative translational energies. The dynamical model employed the quasiclassical trajectory method to calculate the low-pressure limit thermal rate coefficient and hence avoided the use of the usual energy-transfer-based master equation formalism. Except for high temperatures where it is only moderate, the agreement with experiment is found to be good. The disagreement for the high-temperature regimes has been tentatively attributed to rotational effects and the nonthermal behavior near dissociation. Clearly, this issues warrants further investigation.

Acknowledgment. This work has the support of the Fundação para a Ciência e Tecnologia, Portugal, under programs PRAXIS XXI and FEDER (Contract 2/2.1/QUI/408/94).

References and Notes

(1) Holbrook, K. A.; Pilling, M. J.; Robertson, S. H. *Unimolecular reactions*; Wiley: Chichester, England, 1996.

(2) Tsang, W.; Herron, T. *J. Phys. Chem. Ref. Data* **1991**, *20*, 609.

(3) Miller, J. A.; Bowman, C. G. *Prog. Energy Combust. Sci.* **1989**, *15*, 287.

(4) Herzberg, G. *Molecular Spectra and Molecular Structure. III. Electronic Spectra and Electronic Structure of Polyatomic Molecules*; van Nostrand: New York, 1966.

(5) Clary, D. C.; Dateo, C. E.; Stoecklin, T. *J. Chem. Phys.* **1990**, *93*, 7666.

(6) Tao, F.-M.; Drucker, S.; Klemperer, W. *J. Chem. Phys.* **1995**, *102*, 7289.

(7) Klots, T. D.; Dykstra, C. E.; Gutowsky, H. S. *J. Chem. Phys.* **1989**, *90*, 30.

(8) Bouanich, J.-P.; Blanquet, G.; Warland, J. *J. Mol. Spectrosc.* **1995**, *173*, 532.

(9) Lan, B. L.; Bowman, J. M. *J. Chem. Phys.* **1994**, *101*, 8564.

(10) Bowman, J. M.; Padmavathi, D. A. *Mol. Phys.* **1996**, *88*, 21.

(11) Bruehl, M.; Schatz, G. C. *J. Phys. Chem.* **1988**, *92*, 7223.

(12) Lenzer, T.; Luther, K. *J. Chem. Phys.* **1996**, *105*, 10944.

(13) Varandas, A. J. C.; Rodrigues, S. P. J. *J. Chem. Phys.* **1997**, *106*, 9647.

(14) Brown, N. J.; Miller, J. A. *J. Chem. Phys.* **1984**, *80*, 5568.

(15) Gelb, A. *J. Phys. Chem.* **1985**, *89*, 4189.

(16) Varandas, A. J. C.; Pais, A. A. C. C.; Marques, J. M. C.; Wang, W. *Chem. Phys. Lett.* **1996**, *249*, 264.

(17) Gallucci, C. R.; Schatz, G. *J. Phys. Chem.* **1982**, *86*, 2352.

(18) Marques, J. M. C.; Wang, W.; Pais, A. A. C. C.; Varandas, A. J. C. *J. Phys. Chem.* **1996**, *100*, 17513.

(19) Varandas, A. J. C.; Silva, J. D. *J. Chem. Soc., Faraday Trans. 2* **1992**, *88*, 941.

(20) Varandas, A. J. C.; Silva, J. D. *J. Chem. Soc., Faraday Trans. 2* **1986**, *82*, 593.

(21) Varandas, A. J. C. *Adv. Chem. Phys.* **1988**, *74*, 255.

(22) Varandas, A. J. C. *Mol. Phys.* **1987**, *60*, 527.

(23) Schmidt, M. W.; Baldridge, K. K.; Boats, J. A.; Elbert, S. T.; Gordon, M. S.; Jensen, J. H.; Koseki, S.; Matsunaga, N.; Nguyen, K. A.; Su, S. J.; Windus, T. L.; Dupuis, M.; Montgomery, J. A. *J. Comput. Chem.* **1993**, *14*, 1347.

(24) McLean, A. D.; Chandler, G. S. *J. Chem. Phys.* **1980**, *72*, 5639.

(25) Dunning, T. H. *J. Chem. Phys.* **1971**, *55*, 716.

(26) Varandas, A. J. C.; Brandão, J. *Mol. Phys.* **1982**, *45*, 857.

(27) Varandas, A. J. C.; Rodrigues, S. P. J.; Gomes, P. A. J. Manuscript in preparation.

(28) Hippler, H.; Schranz, H. W.; Troe, J. *J. Phys. Chem.* **1986**, *90*, 6158.

(29) Drucker, S.; Cooksy, A. L.; Klemperer, W. *J. Chem. Phys.* **1993**, *98*, 5158.

(30) Bunker, D. L. *Methods Comput. Physics* **1971**, *10*, 287.

(31) Porter, R. N.; Raff, L. M. *Modern Theoretical Chemistry, Dynamics of Molecular Collisions, Part B, Vol. II*; Miller, W. H., Ed.; Plenum: New York, 1976; p 1.

(32) Truhlar, D. G.; Muckerman, J. T. *Atom−Molecule collision theory*; Bernstein, R. B., Ed.; Plenum: New York, 1979; p 505.

(33) Hase, W. L., MERCURY: a general Monte Carlo classical trajectory computer program, QCPE 453. An updated version of this code is VENUS96: Hase, W. L.; Duchovic, R. J.; Hu, X.; Komornik, A.; Lim, K. F.; Lu, D.-H.; Peslherbe, G. H.; Swamy, K. N.; Van de Linde, S. R.; Varandas, A. J. C.; Wang, H.; Wolf, R. J. *QCPE Bull.* **1996**, *16*, 43.

(34) Hase, W. L.; Buckowski, D. G. *Chem. Phys. Lett.* **1980**, *74*, 284.

(35) Stace, A. J.; Murrell, J. N. *J. Chem. Phys.* **1978**, *68*, 3028.

(36) Hase, W. L.; Date, N.; Bhuiyan, L. B.; Buckowski, D. G. *J. Phys. Chem.* **1985**, *89*, 2502.

(37) Bruehl, M.; Schatz, G. C. *J. Chem. Phys.* **1990**, *92*, 6561.

(38) Marques, J. M. C.; Varandas, A. J. C. *J. Phys. Chem.* **1997**, *101*, 5168.

(39) Bentley, J. A.; Huang, C.-M.; Wyatt, R. E. *J. Chem. Phys.* **1992**, *98*, 5207.

(40) Bowman, J. M.; Gadzy, B.; Bentley, J. A.; Lee, T. J.; Dateo, C. E. *J. Chem. Phys.* **1993**, *99*, 308.

(41) Carter, S.; Mills, I. M.; Handy, N. C. *J. Chem. Phys.* **1993**, *99*, 4379.

(42) Marcus, R. A.; Rice, O. K. *J. Phys. Colloid Chem.* **1951**, *55*, 894.

(43) Whitten, G. Z.; Rabinovitch, B. S. *J. Chem. Phys.* **1963**, *38*, 2466.

(44) Whitten, G. Z.; Rabinovitch, B. S. *J. Chem. Phys.* **1964**, *41*, 1883.

(45) Clarke, D. L.; Oref, I.; Gilbert, R. G.; Lim, K. F. *J. Chem. Phys.* **1992**, *96*, 5983.

(46) Varandas, A. J. C.; Wang, W. *Chem. Phys.* **1997**, *215*, 167.

(47) Hase, W. L. *Dynamics of Molecular Collisions, Part B*; Miller, W. H., Ed.; Plenum: New York, 1976; p 121.

(48) Zeiss, G. D.; Meath, W. J. *Mol. Phys.* **1977**, *33*, 1155.

(49) Cummings, F. E. *J. Chem. Phys.* **1975**, *63*, 4960.

(50) Kiefer, J. H.; Mudipalli, P. S.; Wagner, A. F.; Harding, L. *J. Chem. Phys.* **1996**, *105*, 8075.

(51) Tabayashi, K.; Fueno, T.; Takasa, K.; Kajimoto, O.; Okada, K. *Bull. Chem. Soc. Jpn.* **1977**, *50*, 1754.

(52) Roth, P.; Just, Th. *Ber. Bunsen-Ges. Phys. Chem.* **1976**, *80*, 171.

(53) Szekely, A.; Hanson, R. K.; Bowman, C. T. *J. Phys. Chem.* **1984**, *88*, 666.

(54) Szekely, A.; Hanson, R.; Bowman, C. T. *Proceedings of the Thirteenth Symposium on Shock Tubes and Waves*; Treanor, C. E., Hall, J. G., Eds.; SUNY Press: New York, 1982; p 617.